Available online at www.sciencedirect.com
ScienceDirect
International Journal of Heat and Mass Transfer 51 (2008) 5415–5425
International Journal of HEAT and MASS TRANSFER
www.elsevier.com/locate/ijhmt

High heat flux flow boiling in silicon multi-microchannels – Part II: Heat transfer characteristics of refrigerant R245fa

Bruno Agostini [a], John Richard Thome [a,*], Matteo Fabbri [b], Bruno Michel [b], Daniele Calmi [b], Urs Kloter [b]

[a] Heat and Mass Transfer Laboratory (LTCM), École Polytechnique Fédérale de Lausanne (EPFL), CH-1015 Lausanne, Switzerland
[b] IBM Zürich Research Laboratory, Säumerstrasse 4/Postfach, CH-8803, Rüschlikon, Switzerland

Received 14 April 2007
Available online 15 April 2008

Abstract

This article is the second in a three-part study. This second part focuses on flow boiling heat transfer of refrigerant R245fa in a silicon multi-microchannel heat sink and their comparison with the results presented in part I for refrigerant R236fa. This heat sink was the same as utilized in part I. The test conditions covered base heat fluxes from 3.6 to 190 W/cm^2, mass velocities from 281 to 1501 kg/m^2 s and the exit vapour qualities from 0% to 78%. The effect of saturation pressure on heat transfer was tested from 141 to 273 kPa for R245fa and the effect of sub-cooling from 0 to 19 K. The R245fa database includes 693 local heat transfer coefficient measurements, for which four different heat transfer trends were identified, although in most cases the heat transfer coefficient increased with heat flux, was almost independent of vapour quality and increased with mass velocity. The entire database, including both R245fa and R236fa measurements, was compared with four prediction methods for flow boiling heat transfer in microchannels. The three-zone model of Thome et al. (J.R. Thome, V. Dupont, A.M. Jacobi, Heat transfer model for evaporation in microchannels. Part I: presentation of the model, International J. Heat Mass Transfer 47 (2004) 3375–3385) was found to give the best predictions, capturing 90% of the data within ±30% in the slug and annular flow regimes ($x > 5\%$).

Keywords: Flow boiling; Microchannel; High heat flux; Chip cooling; Refrigerant

1. Introduction

The three-zone flow boiling model of Thome et al. [1] for microchannels was developed primarily from single-channel data and did not cover either R245fa or R236fa, nor was data available at very high heat fluxes required for modeling the cooling of microprocessors. As highlighted in part I of the present study, flow boiling in multi-microchannels is of particular interest for electronic cooling applications. This interest comes from several desirable features of micro-evaporator cooling elements as outlined by Agostini et al. [2]. Taking advantage of the latent heat liberated during boiling allows for operation at lower mass flow rates than single-phase cooling and thus can reduce pumping power, resulting in a more energy efficient system. The phase change occurs at constant temperature so that the temperature along the channels is nearly uniform, which is advantageous for thermal interface durability. Furthermore, as shown in part I, the primary heat transfer trend during flow boiling in microchannels is a heat transfer coefficient that increases with heat flux and is mildly dependent on mass velocity, which is very favorable for hot spot management since any localized heat flux increase will result in a limited wall temperature increase. Since the maximum junction temperature allowed for microprocessors is about 85 °C, water cannot be used for this purpose because of its low saturation pressure at a working saturation temperature of about 25 °C, and hydro-fluoro-carbon (HFC) refrigerants are

* Corresponding author. Tel.: +41 21 693 5981; fax: +41 21 693 5960.
E-mail address: john.thome@epfl.ch (J.R. Thome).
URL: http://ltcm.epfl.ch (J.R. Thome).

0017-9310/$ - see front matter © 2008 Elsevier Ltd. All rights reserved.
doi:10.1016/j.ijheatmasstransfer.2008.03.007

Nomenclature

$D_h = 2W \cdot H/(W+H)$	hydraulic diameter (m)
G	mass velocity (kg/m^2 s)
H	channel height (m)
h_{lv}	latent heat of vapourisation (J/kg)
p	pressure (Pa)
q	heat flux (W/m^2)
R_w	wall roughness (nm)
u	velocity (m/s)
W	channel width (m)
x	vapour quality

Greek symbols

α	heat transfer coefficient (W/m^2 K)
δ	liquid layer thickness (m)
μ	dynamic viscosity (Pa s)
ρ	mass density (kg/m^3)
σ	surface tension (N/m)

Subscripts

cr	critical
l	liquid
min	minimal
sat	saturation
v	vapour
w	wall

preferred. However, many refrigerant fluids are available with a large choice of properties so that a suitable fluid for electronics cooling must be chosen. A flow boiling cooling system for electronics must encompass the following constraints: easy servicing with quick connection valves, compatibility with electrical circuitry in case of leaking, high efficiency, low toxicity and a saturation temperature close to ambient. HFCs are generally dielectric, non-flammable and the newest refrigerants have a low toxicity. The use of quick connection valves imposes the use of a low pressure fluid, which is contradictory with a high efficiency since low pressure generally involves a high pressure drop. Taking into account all these constraints, two fluids were selected as good candidates: refrigerant R236fa with a saturation temperature of 25 °C at 282 kPa (studied in part I) and R245fa with a saturation temperature of 25 °C at 149 kPa. No flow boiling data are available in the literature for these two fluids; thus the motivation of the present study is to measure local heat transfer coefficients for R245fa and compare them with R236fa in order to select the better fluid.

The second goal of this study is to select the best prediction method for flow boiling of these refrigerants in microchannels to use for the design of an actual cooling system. Four recent prediction methods for flow boiling heat transfer in microchannels are available in the literature. Thome et al. [1] proposed a model based on the predominance of the elongated bubble flow in microchannels and which states that the main heat transfer mechanism is conduction through the liquid layer around the bubbles. Kandlikar and Balasubramanian [3] proposed a modified version of the Kandlikar [4] correlation for macrotubes. The Lee and Mudawar [5] correlation is based on a non-dimensional analysis of their own heat transfer coefficient measurements in microchannels. Zhang et al. [6] proposed a modification of the Chen [7] correlation.

In the following section, local flow boiling heat transfer coefficient measurements for R245fa will be presented and then compared with those presented in part I. The influence of saturation pressure and sub-cooling will be investigated. Finally, a comparison with the preceding four prediction methods will be presented.

2. Experimental setup and data reduction

As the experimental setup, test section and data reduction procedure are identical to that in part I, refer to part I for details. Experimental conditions and the corresponding uncertainties for the present tests are shown in Table 1.

3. Experimental results on flow boiling heat transfer of R245fa

3.1. Influence of heat flux, mass velocity and vapour quality

Like in part I, 10 mass velocities between 280 and 1500 kg/m^2 s were tested. For each mass velocity, the

Table 1
Operating conditions and measurement uncertainties

	Value	Error
L (mm)	20	±0.02
B (mm)	20	±0.02
N	67	–
W (μm)	223	±10
H (μm)	680	±10
e (μm)	320	±10
$2t$ (μm)	80	±10
D_h (μm)	336	±27
R_w (nm)	170	±50
G (kg/m^2 s)	281–1501	±3%
q_b (W/cm^2)	3.6–190	±5–0.4%
T_b (°C)	23–90	±0.1–1
T_{sat} (°C)	23.7–43.9	±0.1
ΔT_{sub} (K)	0–15	±0.5
p_{in} (kPa)	158–291	±1.5
Δp (kPa)	1.4–125	±0.65
α (kW/m^2 K)	1.8–28.4	±1–30%
x_{out}	0–0.78	±20–0.6%

system pressure was set at 282 kPa and the sub-cooling to 0 K ± 0.5 K. Boiling was first initiated in adiabatic conditions by increasing the flow rate until the inlet orifices produced bubbles by cavitation. Then the lowest heat flux (3.6 W/cm^2) was applied to maintain boiling and the flow rate was reduced to the desired value. The maximum heat fluxes that could be reached with R245fa are lower than those for R236fa since R245fa yielded pressure drops about twice those of R236fa and hence were limited by the capacity of the pump.

Figs. 1–5 show the entire local heat transfer database as a function of the local vapour quality for the 10 different mass velocities at numerous steps in the base heat flux between 3.6 and 189 W/cm^2 to map out the heat transfer trends. The heat transfer coefficients α in the graphs are based on the effective area of the channel, accounting for the fin efficiency as described in part I. Because no pre-evaporator is used in the test loop, the range of vapour qualities is determined by the heat flux. Fig. 6(top), for fixed vapour qualities between 4% and 8%, shows the heat transfer coefficient as a function of the wall heat flux q_w. Fig. 7 shows the local heat transfer coefficient as a function of the local vapour quality for various mass velocities between 281 and 1501 kg/m^2 s for fixed heat fluxes of 17.2 and 100.8 W/cm^2. The heat transfer trends of R245fa are in general close to those of R236fa.

Fig. 1 shows the heat transfer coefficient versus vapour quality at mass velocities of 280.5 kg/m^2 s. At low heat flux ($q < 35.6$ W/cm^2) the heat transfer coefficient increases with vapour quality and increases very little with heat flux,

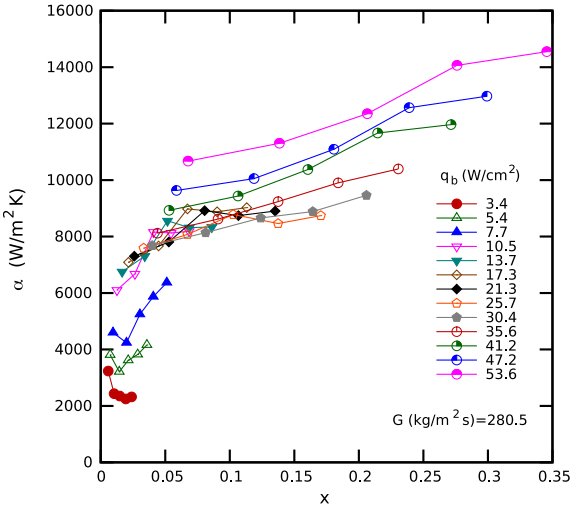

Fig. 1. Local flow boiling heat transfer coefficient versus local vapour quality for increasing base heat fluxes. Mass velocity of 281 and 407 kg/m^2 s.

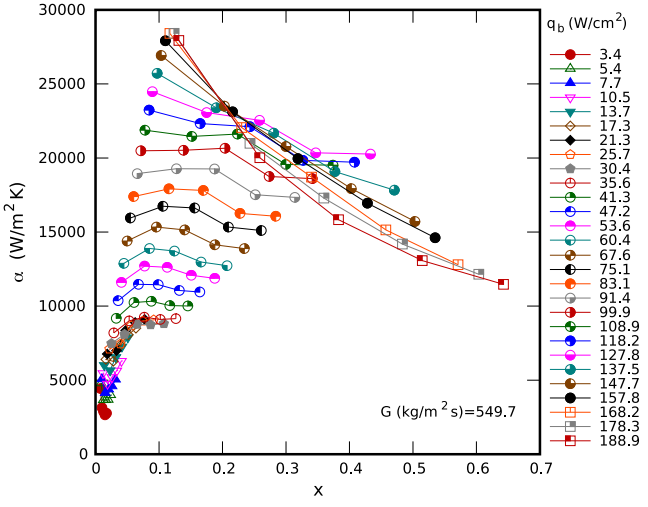

Fig. 2. Local flow boiling heat transfer coefficient versus local vapour quality for increasing base heat fluxes. Mass velocity of 550 and 690 kg/m^2 s.

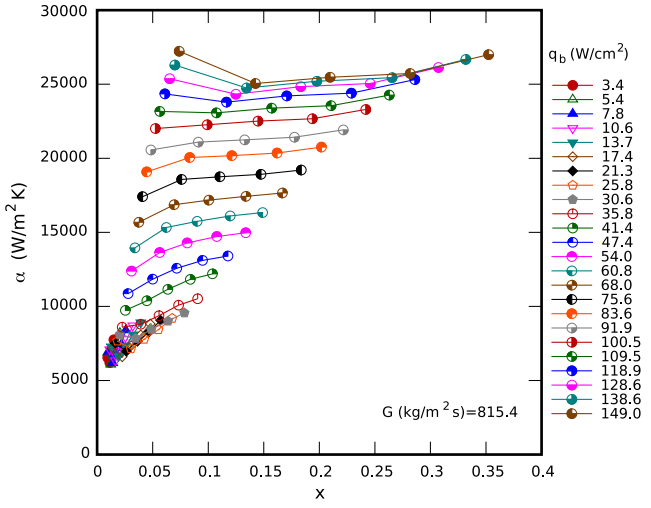

Fig. 3. Local flow boiling heat transfer coefficient versus local vapour quality for increasing base heat fluxes. Mass velocity of 815 and 1001 kg/m^2 s.

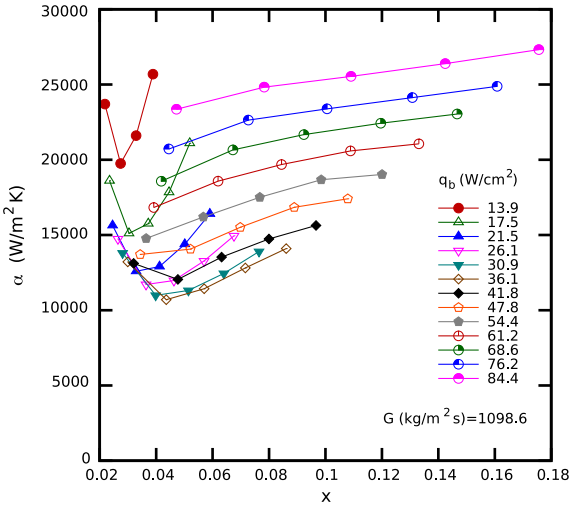

Fig. 4. Local flow boiling heat transfer coefficient versus local vapour quality for increasing base heat fluxes. Mass velocity of 1099 and 1222 kg/m^2 s.

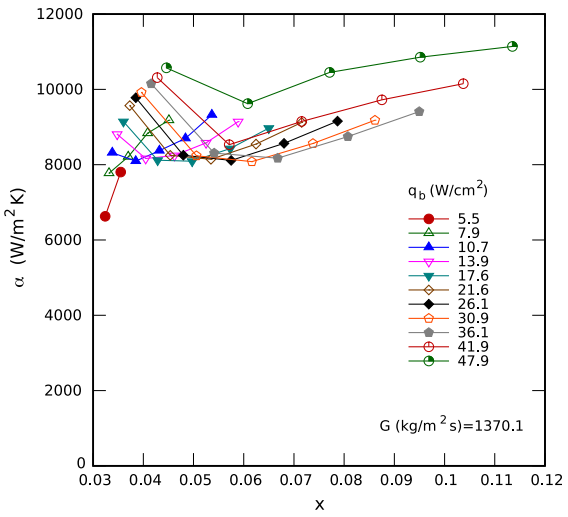

Fig. 5. Local flow boiling heat transfer coefficient versus local vapour quality for increasing base heat fluxes. Mass velocity of 1370 and 1501 kg/m^2 s.

except at the lowest heat fluxes ($q \leqslant 7.7$ W/cm^2) for which the flow is essentially superheated liquid because of the low efficiency of the orifice's flashing effects at low mass velocity. For higher heat fluxes the heat transfer coefficient increases with vapour quality and with heat flux.

Fig. 2 shows the heat transfer coefficient versus vapour quality at mass velocities of 549.7 kg/m^2 s. At low heat flux ($q < 35.6$ W/cm^2) the heat transfer coefficient increases with vapour quality and increases very little with heat flux. For moderate heat fluxes ($35.6 \leqslant q \leqslant 127.8$ W/cm^2, the heat transfer coefficient varies little with vapour quality and increases with heat flux. At higher heat fluxes ($q > 127.8$ W/cm^2), the heat transfer coefficient decreases with vapour quality and heat flux.

Fig. 3 shows the heat transfer coefficient versus vapour quality at mass velocities of 815.4 kg/m^2 s. At low heat flux ($q < 41.4$ W/cm^2) the heat transfer coefficient increases with vapour quality and increases very little with heat flux. For moderate heat fluxes ($41.4 \leqslant q \leqslant 118.9$ W/cm^2 the heat transfer coefficient increases a little with vapour quality but increases with heat flux. For $q > 118.9$ kg/m^2 s, the heat transfer coefficient versus vapour quality is still slightly increasing but is independent of heat flux (this is the transition region before the heat transfer coefficient starts decreasing with heat flux like in Fig. 2).

Fig. 4 shows the heat transfer coefficient versus vapour quality at mass velocities of 1098.6 kg/m^2 s. At low heat flux ($q < 41.8$ W/cm^2) the heat transfer coefficient versus vapour quality has a characteristic U shape and decreases with heat flux. For $q \geqslant 41.8$ kg/m^2 s, the heat transfer coefficient increases slightly with vapour quality and increases with heat flux.

Fig. 5 shows the heat transfer coefficient versus vapour quality at mass velocities of 1370.1 kg/m^2 s. The heat transfer coefficient varies very little with vapour quality and heat flux compared to the figures at lower mass velocities.

Analysis of all these figures leads to the identification of four characteristic trends for R245fa instead of three for R236fa:

(i) At very high heat fluxes ($q_b > 128$ W/cm^2 for $G = 549.7$ kg/m^2 s and $q_b > 137.5$ W/cm^2 for $G = 690.3$ kg/m^2 s), the heat transfer coefficient increases with mass velocity and decreases with increasing heat flux and vapour quality. However, this situation was reached only in Fig. 2 so that no relationship could be found for the transition heat flux at which this behaviour is noticeable, which was able to be done in part I with R236fa.

(ii) At medium heat fluxes ($40 < q_b < 128$ W/cm^2) the heat transfer coefficient is almost constant or slightly increasing with vapour quality and increases with heat flux. Fig. 6 shows that in this region α increases as $q_w^{0.67}$, the same as found for R236fa. The heat transfer coefficient also increases with mass velocity.

(iii) At low vapour quality ($x < 0.1$), low heat flux ($q_b < 40$ W/cm^2) and low to medium mass velocities ($G < 1000$ kg/m^2 s), the heat transfer coefficient increases with vapour quality and is independent of heat flux and mass velocity.

(iv) At low vapour quality ($x < 0.1$), low heat flux ($q_b < 40$ W/cm^2) and high mass velocities ($G > 1000$ kg/m^2 s), the heat transfer coefficient versus vapour quality curve has a characteristic U shape producing a minimum, decreases with increasing heat flux and is independent of mass velocity.

The influence of mass velocity on the heat transfer coefficient at high heat flux is more important for R245fa than for R236fa since increasing the mass velocity by a factor of 2.4 in Fig. 7, the heat transfer coefficient increases by a factor 1.5, while for R236fa the heat transfer coefficient was increased by a factor of only 1.3 when the mass velocity was increased by a factor 5.3. However, at low heat flux, the heat transfer coefficient shows essentially no dependence on mass velocity for both fluids.

Fig. 8 shows a logic diagram of the major heat transfer trends identified for R245fa and R236fa. It can be seen that the trends are very similar for both fluids with two exceptions. For R245fa the heat transfer coefficient is more dependent on mass velocity than for R236fa. Secondly, at high mass velocity and low heat flux, the heat transfer coefficient of R245fa shows a fourth peculiar trend (iv): the U shape with vapour quality and a decrease with increasing heat flux. However, this combination of operational parameters corresponds to very low wall-fluid temperature differences (typically around 1 K) and very low vapour quality (less than 5%) where the experimental uncertainty is the highest (±30%). Furthermore, heat transfer coefficients measured for low q, low x and high G are likely to be influenced by the bubbles generated by the inlet orifice by cavitation. As for R236fa, trend (i) matches with a sharp increase in fluctuations of the wall temperature, which

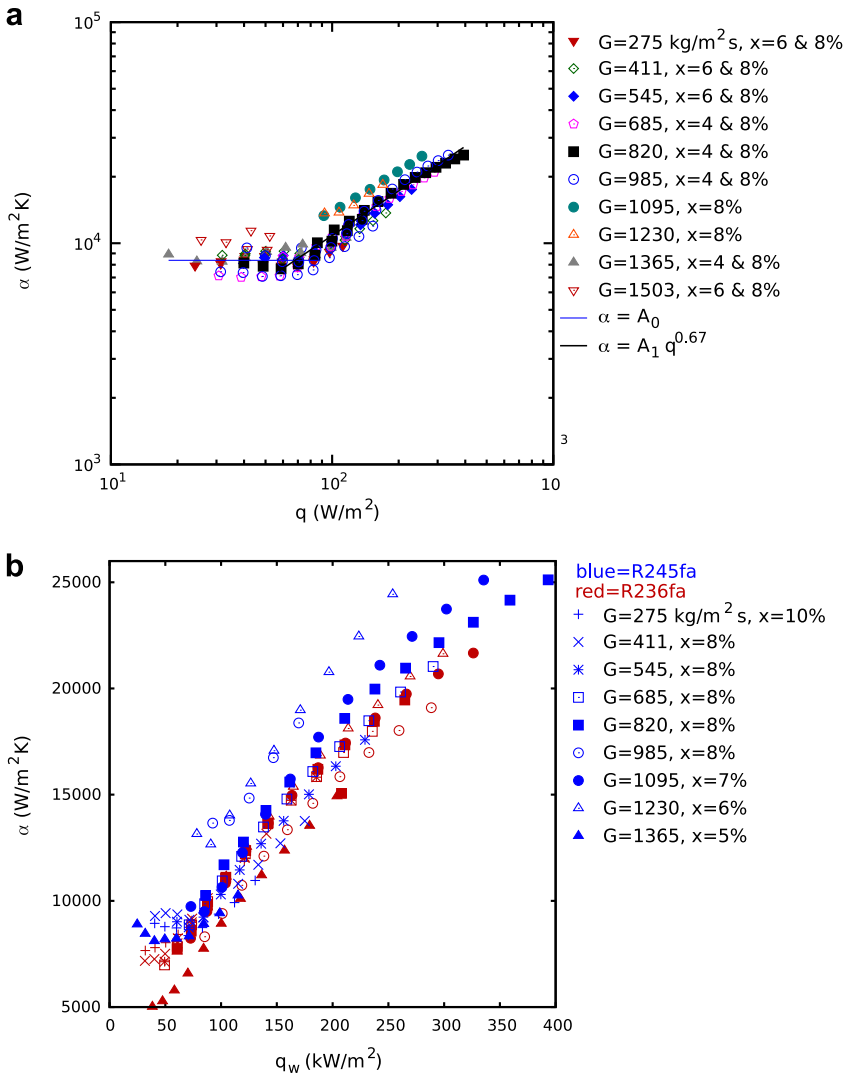

Fig. 6. Flow boiling heat transfer coefficient versus channel wall heat flux at low vapour quality: (a) R245fa only and (b) comparison between R245fa (blue) and R236fa (red). (For the interpretation of color in this figure legend, the reader is referred to the Web version of this article.)

might be explained by the onset of intermittent dry-out. As a consequence, three significant trends can be identified in parts I and II of the present study:

(1) at low heat flux, α increases with x and is independent of q and G;
(2) at medium heat flux, α increases with q, is independent of x and increases slightly with G (R245fa) or is independent of G (R236fa);
(3) at high heat flux, α decreases with increasing q and x and increases with G.

3.2. Influence of saturation pressure

The influence of the saturation pressure on the heat transfer coefficient was measured for saturation pressures between 144 and 273 kPa (i.e., saturation temperatures from 23.8 to 42.6 °C) at a mass velocity of 1001 kg/m^2 s, a base heat flux of 18 W/cm^2 and a sub-cooling of 0 K for R245fa and between 185 and 311 kPa (i.e., saturation temperatures from 14 to 29 °C) at a mass velocity of 811 kg/m^2 s, a base heat flux of 81 W/cm^2 and a sub-cooling of 0 K for R236fa. The operating conditions (mass velocity and heat flux) for R245fa and R236fa are different because the test facility is limited by pressure drop, which is very different for each fluid. Fig. 9 shows the local heat transfer coefficient versus local vapour quality for four different saturation temperatures for R245fa (a) and R236fa (b), with their uncertainties indicated by the size of the data point symbol. The influence of the saturation pressure on the heat transfer coefficient is obvious for R236fa. The heat transfer coefficient increases with pressure and is correlated with

$$\alpha = 87,645 \cdot \left(\frac{p}{p_{cr}}\right)^{0.67} \quad (1)$$

where p is the saturation pressure and p_{cr} is the critical pressure with a correlation coefficient R^2 of 0.99. The influ-

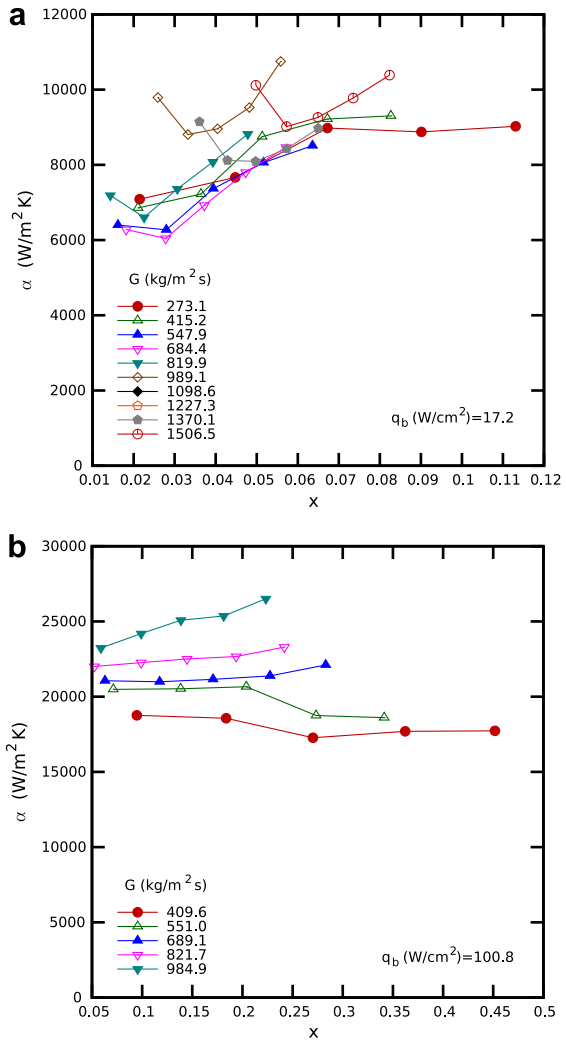

Fig. 7. Flow boiling heat transfer coefficient versus local vapour quality for increasing mass velocities, for base heat fluxes of 17.2 and 100.8 W/cm^2.

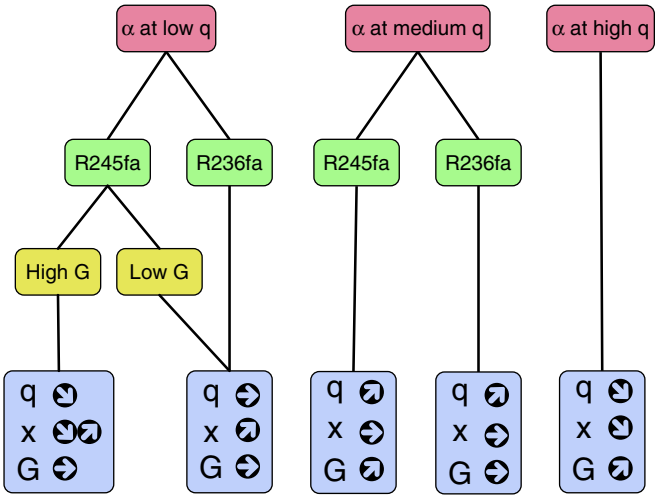

Fig. 8. Heat transfer trends identified in the present study for R245fa and R236fa: the arrows show the effect of the parameters q, x and G on α, either increasing (↗), decreasing (↘) or no effect (→) on α.

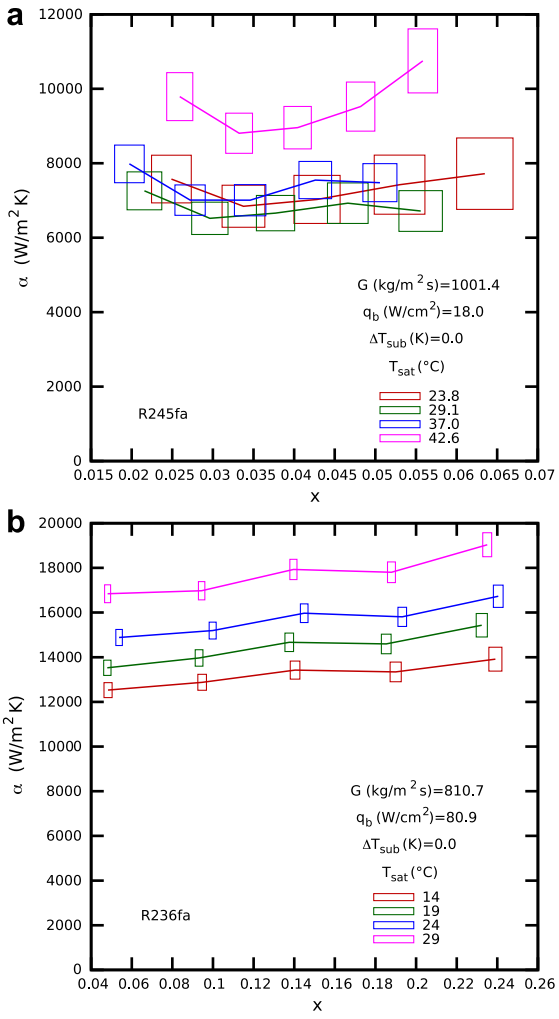

Fig. 9. Influence of saturation temperature on the local heat transfer coefficient for refrigerant: (a) R245fa and (b) R236fa.

ence of saturation pressure is less obvious for R245fa. The heat transfer coefficient is the same for saturation temperatures of 23.8 and 29.1 °C, increases slightly for 37 °C and is much larger for 42.6 °C. Thus, the trend is an increase of the heat transfer coefficient with pressure, but because of the higher pressure drop for R245fa, its measurements were made at a much lower heat flux, resulting in a much lower wall to fluid temperature difference and therefore a much higher uncertainty, which may explain the less definite trend.

3.3. Influence of sub-cooling

The influence of the sub-cooling on the heat transfer coefficient was measured for sub-coolings between 0.6 and 18.3 K at a mass velocity of 1001 kg/m^2 s, a base heat flux of 38.1 W/cm^2 and a saturation temperature of 38.1 °C for R245fa and between 0 and 19 K at a mass velocity of 811 kg/m^2 s, a base heat flux of 134 W/cm^2 and a saturation temperature of 25 °C for R236fa. These heat fluxes were chosen so that the onset of boiling was reached even

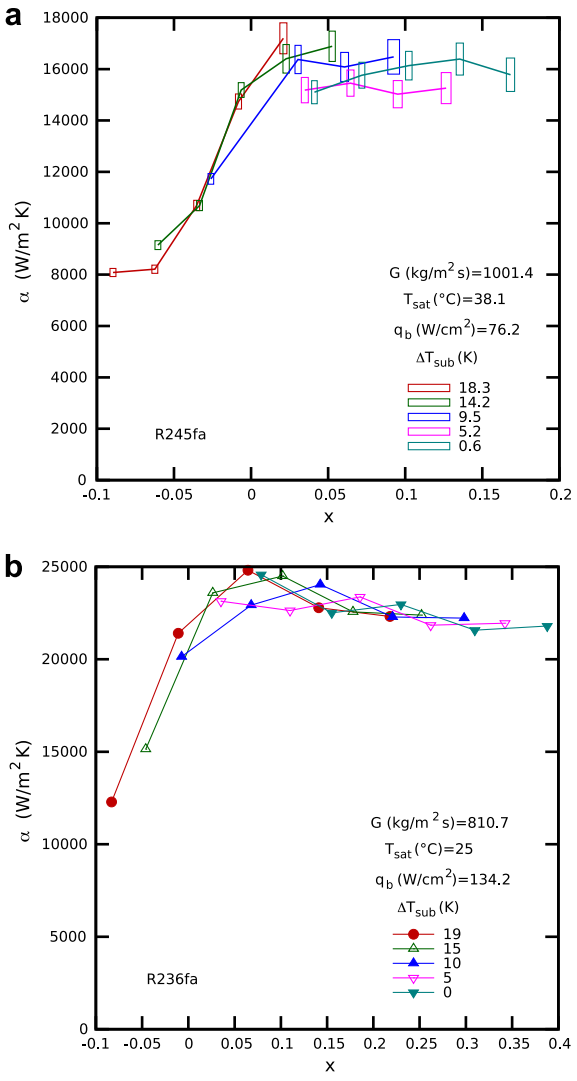

Fig. 10. Influence of sub-cooling on the local heat transfer coefficient for refrigerant: (a) R245fa and (b) R236fa.

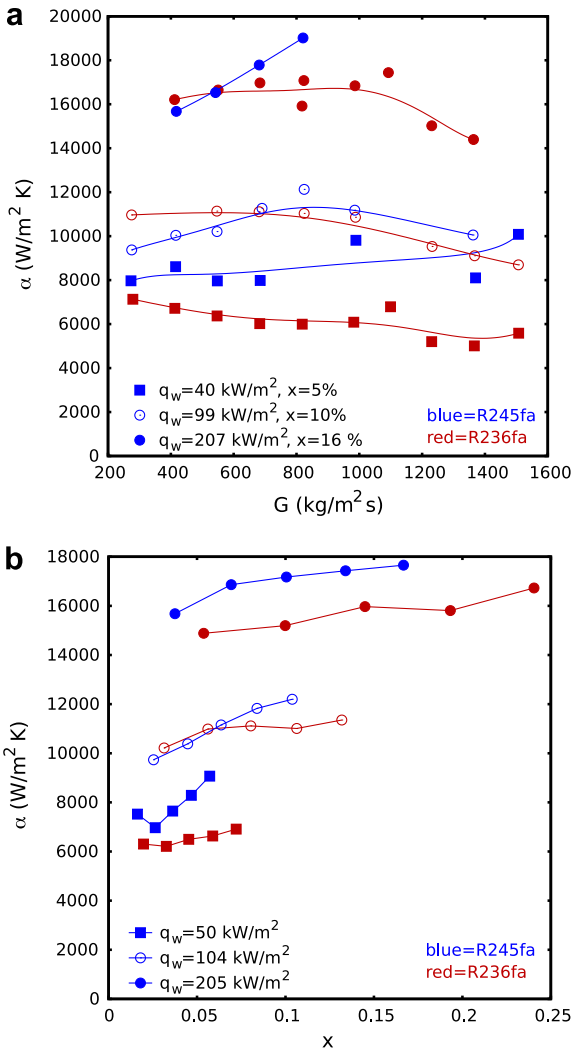

Fig. 11. Comparison between R245fa (blue on Web) and R236fa (red on Web) heat transfer coefficient: (a) heat transfer coefficient versus mass velocity for three fixed heat fluxes at low vapour quality; (b) local heat transfer versus local vapour quality for three fixed heat fluxes and $G = 815$ kg/m^2 s.

at the largest sub-cooling. Fig. 10 shows the local heat transfer coefficient versus local vapour quality for five different sub-coolings for R245fa with uncertainties (a) and for R236fa without (b). There is not much downstream effect of the level of sub-cooling on the heat transfer coefficients in the saturated region. On the other hand, sub-cooled flow boiling heat transfer coefficients fall off with increasing sub-cooling.

4. Comparison with R236fa

A graphical comparison of R245fa versus R236fa is shown in Fig. 11(a).[1] It compares the heat transfer coefficient versus mass velocity for R245fa (blue/dark) and R236fa (red/gray) at a fixed vapour quality for three different base heat fluxes of 40, 99 and 207 W/cm^2. In Fig. 6(b), the comparison shows the heat transfer coefficient versus the wall heat flux for a fixed vapour quality and mass velocities between 275 and 1365 kg/m^2 s for R245fa and R236fa. Fig. 11(b) compares the local heat transfer coefficient versus local vapour quality for R245fa and R236fa at a fixed mass velocity of 815 kg/m^2 s for three different base heat fluxes of 50, 104 and 205 W/cm^2. Table 2 shows the heat flux averaged ratio between the heat transfer coefficients of R245fa and R236fa for the different mass velocities corresponding to Fig. 6. Heat transfer of R245fa is lower than for R236fa at low mass velocities ($G < 685$ kg/m^2 s) and larger at high mass velocities ($G \geqslant 685$ kg/m^2 s). The ratio $\alpha_{R245fa}/\alpha_{R236fa}$ increases with mass velocity and ranges from 0.90 to 1.37 and is 1.07 in average. Thus, it can be concluded that the heat transfer performance of R245fa is slightly but not significantly higher than that of R236fa. Fig. 11(a) also highlights that for R236fa the mass

[1] For the interpretation of color in this figure, the reader is referred to the Web version of this article.

Table 2
Comparison of R245fa and R236fa heat transfer coefficients as a function of mass velocity

G (kg/m^2 s)	$\alpha_{R245fa}/\alpha_{R236fa}$
275	0.90
411	0.93
545	0.97
685	1.01
820	1.04
985	1.37
1095	1.10
1230	1.24
1365	1.07

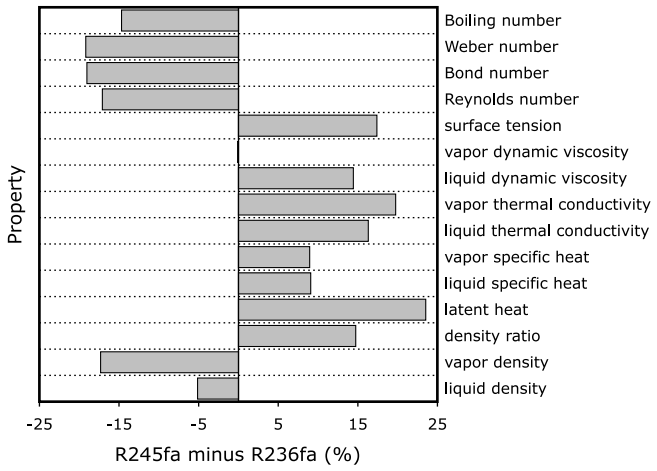

Fig. 12. Comparison of the thermophysical properties of R236fa relative to those of R245fa. The x-axis represents the value in percent of the difference between the properties of R245fa and those of R236fa.

velocity dependence of the heat transfer coefficient is very low while it is more notable for R245fa, for which no explanation is presently available but could be related to the dynamics of elongated bubble flow since the thermophysical properties of the two fluids are quite different as shown in Fig. 12. This figure shows a comparison of the thermophysical properties of R236fa relative to those of R245fa. The x-axis represents the value in percent of the difference between the properties of R245fa and those of R236fa. Notably all the non-dimensional numbers important for two-phase flow are between 15% and 20% lower for R245fa, suggesting that the bubbles dynamics might be indeed significantly different.

5. Comparison with prediction methods

The present database was compared with four prediction methods for flow boiling heat transfer in microchannels, namely those of Thome et al. [1], Kandlikar and Balasubramanian [3], Lee and Mudawar [5] and Zhang et al. [6]. Data for vapour qualities larger than 5% were selected so that the corresponding heat transfer coefficients are not influenced by the orifices and the 90° turn of the flow at the inlet. As a consequence, the database contains 1438 local heat transfer coefficients for R245fa and R236fa.

The Thome et al. [1] three-zone model uses three parameters representative of the microscale heat transfer mechanisms. This model considers that there are three main heat transfer mechanisms in microchannels: (1) transient heat conduction through the liquid layer confined around passing bubbles, (2) convection to the passing liquid slugs and (3) convection to the vapour if the liquid layer in (1) dries out. The predictions of this model depend mainly on three parameters: bubble formation frequency, the initial liquid layer thickness at the bubbles's nose and the minimum liquid layer thickness at dry-out. These parameters cannot be calculated and thus need to be optimized from its database. This work was done by Dupont et al. [8] on a large heat transfer coefficient database including 1491 data points for seven fluids from seven independent laboratories. The same empirical coefficients were used in the present comparison, except for the minimum liquid layer thickness at dry-out, which should be about equal to the wall roughness, and the latter used when known. In the present study, the wall roughness (maximum peak amplitude, shown in Fig. 13) was measured from scanning electron microscope images and was found to vary from 100 to 200 nm with an average of 170 nm from 15 measurements. Thus, the latter value was used here for the minimum liquid layer thickness δ_{min} in the three-zone model here (original value was 300 nm). Furthermore, the three-zone model is implemented using the equivalent diameter, i.e., the diameter of a circular tube yielding the same cross-sectional area as the rectangular channel, defined as $D_e = \sqrt{4/\pi \cdot W \cdot H}$ to calculate the mass velocity. The heat flux based on the effective area (accounting for the fin efficiency as in part I) is input into the three-zone model. The correlation of Kandlikar and Balasubramanian [3] is based on a superposition method including a nucleate boiling and a convective

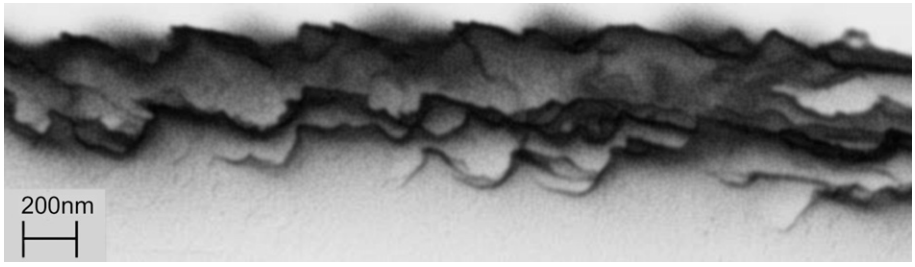

Fig. 13. SEM view of etched silicon roughness.

Table 3
Comparison of data with prediction methods

Method	% of data within ±30%			Mean absolute error (%)			Mean relative error (%)		
	R245fa	R236fa	All	R245fa	R236fa	All	R245fa	R236fa	All
[1]	86	93	90	17	19	18	−5	12	4
[3]	58	57	58	30	34	32	14	−30	−23
[5]	0.1	0	0.1	584	633	612	−583	−629	−609
[6]	18	30	25	48	44	46	44	28	35
Data points	631	813	1442						

boiling contribution, like macroscale methods, with coefficients and exponents optimized using a microchannel heat transfer database. Lee and Mudawar [5] proposed a method based on three contributions, each corresponding to a vapour quality range (0–0.05, 0.05–0.55 and 0.55–1). Each of the three equations is based on a single-phase flow expression (Nusselt or Dittus–Boelter) and is modified with a Martinelli parameter, a Boiling number or a Weber number to predict the flow boiling heat transfer coefficient. The Zhang et al. [6] method is a modified version of the classic Chen [7] correlation, but accounts also for laminar flows in microchannels and uses a modified Reynolds number.

Table 3 shows that the best prediction model is the three-zone model with 90% of the data predicted within ±30%, a mean absolute error of 18% and a mean relative error of 4%. Using the original roughness of 300 nm as in Dupont et al. [8], the corresponding values are 31%, 38% and 37%, indicating the sensitivity of boiling in microchannels to the surface roughness. The Lee and Mudawar [5] method does not perform well, but the comparison cannot be done correctly here because they used the mean base heat flux in their method instead of the local wall heat flux. As they used a copper heat sink, their wall heat fluxes are probably very different from the present ones with silicon for the same base heat flux. The method of Kandlikar and Balasubramanian [3] did not extrapolate to these two fluids very well either. The Zhang et al. [6] method largely underpredicted the data. This is probably due to the fact they used the same boiling suppression factor as in the original Chen [7] correlation, which does not account for the

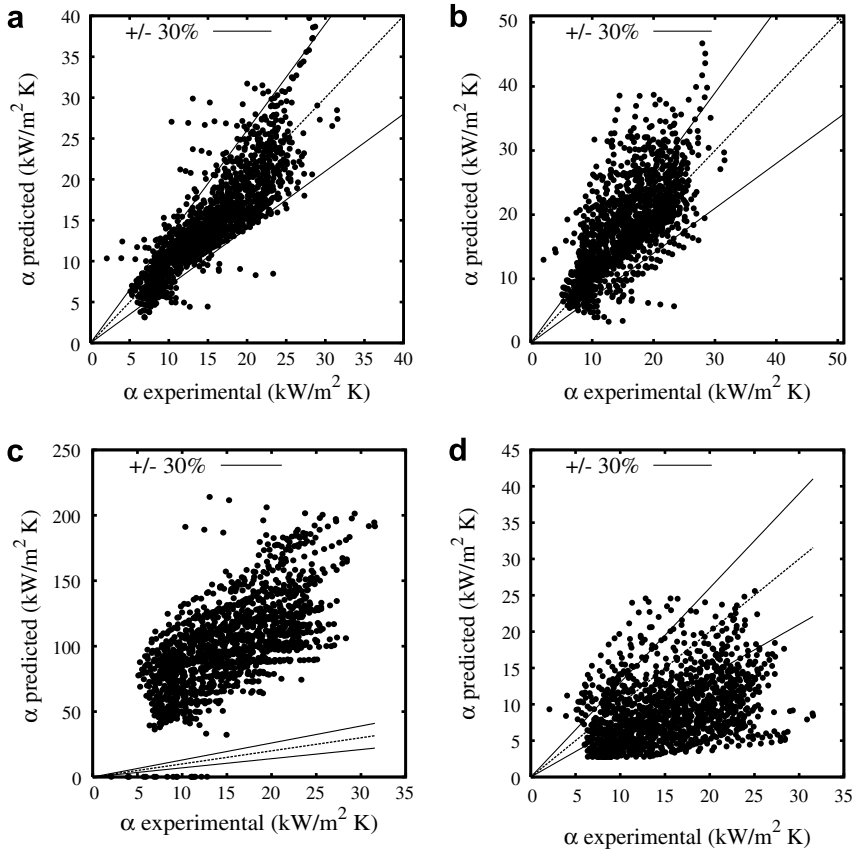

Fig. 14. Comparison between the present database of local heat transfer coefficients and four prediction methods for flow boiling heat transfer in microchannels: (a) Thome et al. [1], (b) Kandlikar and Balasubramanian [3], (c) Lee and Mudawar [5] and (d) Zhang et al. [6].

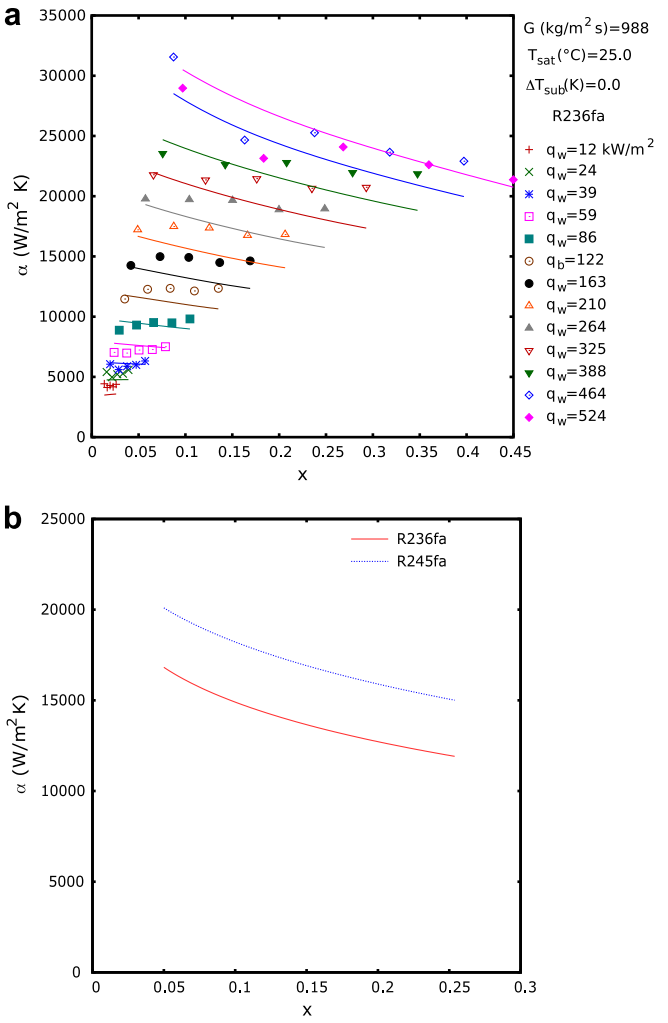

Fig. 15. (a) Comparison between the heat transfer coefficient versus vapour quality curve measured in the present study and that predicted by the three-zone model for increasing wall heat fluxes, refrigerant R236fa and $G = 988\ \mathrm{kg/m^2\,s}$. (b) Comparison of the heat transfer coefficients predicted by the three-zone model for R236fa and R245fa.

predominance of heat flux dependent heat transfer coefficients during flow boiling in microchannels compared to macrotubes. Fig. 14 shows the respective error plots of the four methods. Fig. 15(a) shows a representative comparison of the three-zone model to one set of test data. The three-zone model is seen to quantitatively capture the trends of α versus x but not the exact trends. Also, the three-zone model cannot so far capture all the trends described in Fig. 11, even though statistically this model works quite well.

Fig. 15(b) shows a simulation of the heat transfer coefficient versus vapour quality predicted by the three-zone model for R236fa and R245fa at a mass velocity of $800\ \mathrm{kg/m^2\,s}$, a wall heat flux $200\ \mathrm{kW/m^2}$ and a pressure of 282 kPa. The three-zone model predicts higher heat transfer coefficients for R245fa compared to R236fa, which is in agreement with the present experimental data. For these conditions, the heat transfer coefficient predicted by three-zone model for R245fa is 25% higher than that of R236fa, while it was measured to be only 11% higher for the same conditions. It is clear that further improvements are required to the three-zone model to capture additional characteristics of the flow and their influence on heat transfer.

6. Conclusions

Local heat transfer coefficients were measured for R245fa flow boiling in a silicon multi-microchannel heat sink for a large range of heat fluxes, mass velocities and vapour qualities and were compared with the measurements for R236fa presented in part I. Three significant heat transfer trends were identified. At low heat flux, the heat transfer coefficient increases with vapour quality and is independent of heat flux and mass velocity. At medium heat flux, the heat transfer coefficient increases with heat flux as $q^{0.67}$, is independent of vapour quality, increases slightly with mass velocity for R245fa or is independent of mass velocity for R236fa. At high heat flux, the heat transfer coefficient decreases with increasing heat flux and vapour quality and increases with mass velocity. The heat transfer coefficient was found to increase with saturation pressure, particularly for R236fa and the level of sub-cooling was found to have no influence for saturated boiling, while sub-cooled boiling data were below those for saturated boiling, similar to other previous studies. The present database, including 1438 local heat transfer coefficients for both fluids, was compared with four prediction methods for flow boiling heat transfer in microchannels. The three-zone model of Thome et al. [1] was found to be the best and predicted 90% of data within ±30% when setting the minimum film thickness to the measured channel roughness. Furthermore, the three-zone model also predicts higher heat transfer coefficients for R245fa compared to R236fa, which is in agreement with our measurements.

Acknowledgements

The authors wish to thank the Swiss Federal Office for Professional Education and Technology (KTI) for sponsoring this work under contract no. 6862.2 DCS-NM and for providing the financial support for Dr. Agostini in this project. The authors also wish to recognize the support of the IBM Zürich research center for the construction of the test facility and the fabrication of the test sections. The authors wish to thank Honeywell for providing the R245fa for the tests.

References

[1] J.R. Thome, V. Dupont, A.M. Jacobi, Heat transfer model for evaporation in microchannels. Part I: presentation of the model, Int. J. Heat Mass Transfer 47 (2004) 3375–3385.

[2] B. Agostini, M. Fabbri, J.E. Park, L. Wojtan, J.R. Thome, B. Michel, State-of-the-art of high heat flux cooling technologies, Heat Transfer Eng. 28 (4) (2007) 258–281.

[3] S.G. Kandlikar, P. Balasubramanian, An extensions of the flow boiling correlation to transition, laminar, and deep laminar flows in mini-channels and microchannels, Heat Transfer Eng. 25 (3) (2004) 86–93.
[4] S.G. Kandlikar, A general correlation for saturated two-phase flow boiling heat transfer inside horizontal and vertical tubes, J. Heat Transfer 112 (1990) 219–228.
[5] J. Lee, I. Mudawar, Two-phase flow in high-heat-flux microchannel heat sink for refrigeration cooling applications: Part II—Heat transfer characteristics, Int. J. Heat Mass Transfer 48 (2005) 941–955.
[6] W. Zhang, T. Hibiki, K. Mishima, Correlation for flow boiling heat transfer in mini-channels, Int. J. Heat Mass Transfer 47 (2004) 5749–5763.
[7] J.C. Chen, Correlation for boiling heat transfer to saturated fluids in convective flow, Ind. Eng. Chem. Process Design Dev. 5 (3) (1966) 322–329.
[8] V. Dupont, J.R. Thome, A.M. Jacobi, Heat transfer model for evaporation in microchannels. Part II: comparison with the database, Int. J. Heat Mass Transfer 47 (2004) 3387–3401.